

Chapter 12

THE RATE MODULATION OF CELL AND TISSUE FUNCTION VIA ELECTROCHEMICAL INFORMATION TRANSFER

ARTHUR A. PILLA

Introduction

THAT BIOLOGICAL SYSTEMS exhibit remarkable sensitivity to weak electrical currents is now without question. Some organisms (1) have developed sensitivities to D.C. voltage fields on the order of 10^{-7} V/cm. The *application* of weak currents to elicit changes in growth patterns appears to have first been performed by developmental biologists in tissue regeneration studies (2-4). This was followed by the studies of orthopedists and bone physiologists who showed that the adaptive response of bone to mechanical stresses could involve an electrical step via the known strain generated potential characteristics (5-10).

The facts now are that a variety of living cells have been shown to be capable of functional response to weak electrical current. It has been reported that D.C. current in bone will produce osteochondrogenesis (11-14) as well as bacteriostasis (15). Capacitively coupled currents cause increased *in vitro* DNA synthesis (16, 17) and affect the growth of explanted bone rudiments (18). Inductively coupled pulsating current stimulates increased DNA synthesis in isolated bone cells (19); modulates the rate of amphibian RBC response to trauma (with resultant DNA uncoiling) (20, 21), of fracture healing in the rat (22), and of limb regeneration in the salamander (23); and has been successfully employed clinically for non-unions and pseudarthroses of bone (24-26). Radiofrequency modulated at low frequencies (1000 Hz) has been reported to affect Ca^{++} uptake in isolated cerebral tissue (27, 28) and learning ability in primates (29).

This study reviews and relates the real-time electrochemical response of living cells to weak currents to biological regulatory activity. It is shown that the specific interactions of simple ions at the cell surface can provide the basis of a kinetic electrochemical information approach by which cell function can be modulated (30-36).

Electrochemistry at the Cell Surface

In order for the living cell to exhibit a functional response to electrical

perturbation it is necessary that this perturbation actually reach the cell. In contrast to voltages (and associated currents) that are applied directly across the cell's plasma membrane, the situation considered in this study involves creating voltage gradients within a macro portion of tissue such that both "terminals" of the gradient are extracellular. Considering that cells are surrounded by highly conducting ionic medium (i.e. a very poor dielectric), it is clear that a voltage field containing relatively low frequencies (<100 mHz) can only exist if current flows. The above situation places certain constraints upon the characteristics of both the cell/tissue complex and the applied electricity. Generally, two main situations prevail, dependent upon whether current crosses the cell surface or remains extracellular. The cell membrane's electrical impedance determines the parameters of the electrical perturbation necessary for either of the above to exist.

The first step therefore is to characterize the impedance of the individual cell membrane. This has been carried out using an electrochemical kinetic approach, which is described in detail elsewhere (31, 34, 36). For the purposes of this study it is necessary to recall that the plasma membrane (and other organelle) surfaces exhibit electrical charge separation giving it capacitorlike properties. The structure of this capacitor is determined primarily by the interactions of water dipoles and hydrated ions with the charged chemical groups associated with the various lipid, protein, and carbohydrate components of the membrane. In addition, this capacitor is leaky since transmembrane ion transport occurs. These general properties represent a class of electrochemical processes that characterize and govern the passage of current across the cell membrane. The following electrochemical steps were modelled and subsequently verified in amphibian epithelial (34, 37) and human red blood (38) cells:

- a. Dielectric charge storage due to the asymmetrical molecular organization (one-sidedness) of most membrane structures. This physical process can be represented by a simple capacitor (see a, Fig. 12-1).
- b. Finite rate ion or dipole building at specific molecular sites on the aqueous interfaces of the cell surfaces. The kinetics of this step can be represented by a series resistor/capacitor combination if uncoupled from membrane transport (see b, Fig. 12-1) or by a parallel resistor/capacitor combination if part of the latter.
- c. Transmembrane ion transport with finite entry (partitioning) kinetics. This two-step process can be represented by a resistor (for entry kinetics) in series with a parallel resistor/capacitor combination (for the transport portion — see c, Fig. 1).

Consideration of all of the above shows that current can cross the cell membrane via a complex, but readily discernible, set of electrochemical steps that have been shown to be representative of the cell's real-time

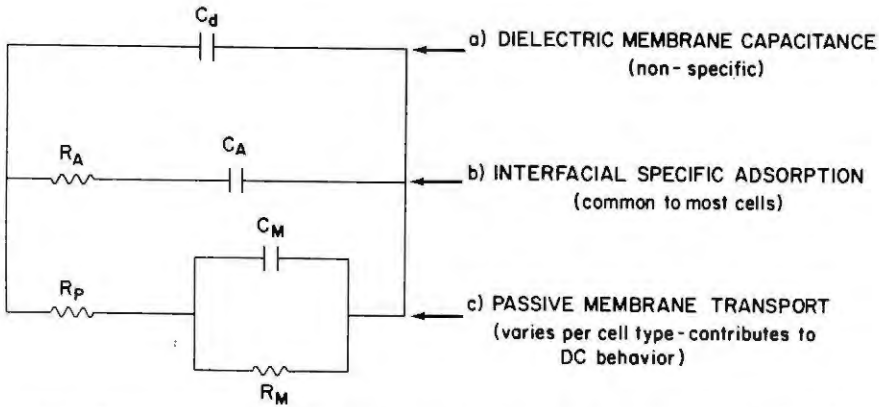


Figure 12-1. Generalized aperiodic equivalent electric circuit representing the nonfaradaic electrochemical kinetics of the three major types of current pathways at cell surfaces. All capacitors represent the average concentrations of ions, dipoles, and charged functional groups at the aqueous interfaces. All resistors represent the kinetics of interaction of these charged species. Note that passive membrane transport is considered a two-step process represented by entry (partitioning) kinetics (R_p) in series with an ion transfer relaxation process (R_M/C_M).

interaction with its charged environment. Impedance measurements that have been thus far carried out have allowed the relative magnitudes of the time constants (relaxation times) of these processes to be determined. As expected, dielectric and specific adsorption time constants are somewhat smaller (1-100 μ sec) than those involving membrane transport (1-100 msec). Of importance also is the observation from these and other (39-45) studies that the steady stage (D.C.) current pathway (due to transport) exhibits a specific resistivity several orders of magnitude above that of the extracellular fluid.

In addition to the above it is necessary to point out that a portion (albeit small) of the charges accumulated at the extracellular surface are mobile and can be displaced by mechanical and thermal forces. For example, cell electrophoresis is caused by the passage of sufficient levels of D.C. current (approx. 1 V/cm developed electric field) to displace these mobile charges from their equilibrium point with respect to the cell's outer surface. This allows the cell to exhibit a net negative charge and migrate to the positive electrode (anode). At the cellular level it is also possible, when the cell is in a fixed position (immobile as in a tissue) to achieve a potential along (as opposed to across) the cell surface. Once again the field required to achieve significant charge displacement would be of the order of 1 V/cm, which, using typical solution resistivities, necessitates at least 1 mA/cm² of D.C. current.

From a very general viewpoint, therefore, electrochemical processes involving charge displacement along, at, or across the cell surface can all

respond to electrical current input. It cannot be too heavily emphasized that the range of relaxation times of these phenomena necessitates a current flow in the presence of an externally applied electric field for a significant perturbation to exist. This, of course, results from the relatively high conductivity of the extracellular medium. In addition, significant charge displacement along the cell's surfaces requires several orders of magnitude higher D.C. current than that which is required to modulate transmembrane ion passage or that which is present as an average value in the pulsating current required to couple to dielectric or specific adsorption steps.

A detailed analysis of all of the above charge interactions at cell surfaces and junctions (36) has resulted in the following postulates:

- a. Charge interactions involving the basic dielectric structure of the cell membrane are governed by electrostatics and therefore are not specific. Electric coupling to this relaxation process is not predicted to have functional consequences.
- b. Potential dependent specific adsorption at any cell surface involves physicochemical interactions, which provide ionic and molecular specificity. Perturbation of this process is anticipated to be of significant functional consequence to the cell.
- c. Transmembrane ion transport involves selective processes and is often under enzymatic control in order to maintain correct intracellular ionic concentrations for the cell's functional activity versus cycle stage. Electrical modulation of this process is of obvious importance of cell function and can occur via specific adsorption steps (most likely) or directly (less likely since cell membranes rarely behave like simple ion selective electrodes).

If electrochemical processes at the cell surface are important steps in cell regulation, it is possible to consider the choice of current waveform parameters in terms of an informational approach, as opposed to one in which energy is the primary factor. Electrical coupling to these processes can be achieved by sufficient excitation of their kinetics for which some data are available. In addition, it is clear that the kinetics and mechanisms of cell surface electrochemistry require a periodic perturbation to exhibit a net change versus the resting or "steady state" condition. To illustrate this consider the following generalized model. Current that perturbs a specific adsorption process (i_A) is a function of changes in potential (ΔE) and in surface concentration ($\Delta\Gamma$) of the adsorbing species, i.e.

$$i_A = f(E, \Gamma) \quad (1)$$

If the system behaved in a purely linear fashion then the explicit relation of i_A to these parameters would be

$$i_A = I_F \Delta E + I_T \Delta \Gamma \quad (2)$$

where I_E and I_Γ are coefficients respectively representing the potential and concentration dependence of the adsorption process. Equation 2 has been employed (31) to describe the time constant (kinetics) of the specific adsorption process (experimentally) verified on amphibian epithelial and human RBC systems as indicated (above). It is a basic property of such kinetic systems to exhibit nonlinearity due to, for example, a difference in forward (adsorption) and reverse (desorption) rate constants. A convenient expression of this is to continue the expansion of equation 1 beyond the linear terms (equation 2). This gives

$$i_A = I_E \Delta E + I_\Gamma \Delta \Gamma + \frac{1}{2}(I_E^2 \Delta E^2 + I_\Gamma^2 \Delta \Gamma^2) \quad (3)$$

where cross products have been neglected and in which I_E^2 and I_Γ^2 are coefficients representing the second derivatives of the potential and concentration dependence of specific adsorption respectively. The contribution of the nonlinear terms to the response of this process to periodic current input will result in a net drift in the surface concentration of the adsorbing species to a new resting value. This surface concentration shift will not be observed with nonrepetitive pulse inputs, thereby allowing the linear impedance to be determined. The degree of nonlinearity (irreversibility) depends upon the amplitude of the basic perturbation. For the weak current situation considered here it would not be expected to exceed 10 percent.

A rationale for the choice of parameters of periodic current waveforms can now be set forth. A first requirement is to couple to the basic kinetics of the cell surface electrochemical process. Originally, the prediction was made, drawing upon electrochemical experience at other charged interfaces, that pulse widths narrower than 1-10 μ sec would not efficiently couple to the desired kinetics. The basic reason for this is that for a pulse width (τ), much shorter than the relaxation time of the desired receptor process (τ_A) the pulse amplitude requirement would rapidly rise, even for a periodic signal having a duty cycle of 2. This can compromise selectivity, as will be shown below. In addition, it is important to consider the presence of the highly conducting extracellular fluid that, for most cells, will represent a shorting current pathway as the pulse width is increased. To illustrate this, the following simple model can be employed. The impedance of a cell membrane at which specific adsorption occurs is given by:

$$Z_A = R_A + 1/C_A s \quad (4)$$

for which the aperiodic equivalent circuit is as shown in b, Fig. 12-1. Here R_A represents the kinetics of the binding process, C_A the average concentration of the adsorbing species, and s is complex frequency ($s = \sigma + j\omega$). Examination of equation 4 shows that, as frequency decreases (pulse width increases), Z_A becomes very large prohibiting further current flow. If the

whole cell is considered bathing in conducting extracellular medium, equation 4 becomes:

$$\frac{1}{Z_T} = \frac{1}{R_e + \frac{1}{C_d s + 1/(R_A + 1/C_A s)}} + \frac{1}{R_L} \quad (5)$$

which shows that the total impedance (Z_T), is now a function of the cytoplasmic resistive pathway (R_e) and the leak pathway (R_L), as well as the dielectric membrane capacitance (C_d). This equation represents the equivalent electric circuit shown in Figure 12-2. It can readily be seen that as $s \rightarrow 0$ (pulse width increases) current ultimately flows solely through R_L . This is of no consequence to the cell under the weak current conditions considered (i.e. electrokinetic phenomena are not significantly perturbed). It would therefore appear inefficient to utilize a basic pulse width significantly longer than the time constant of the cell surface electrochemical process supposed involved in cell regulation. Basic pulse durations between 10 and 1000 μsec would therefore be predicted to most optimally couple to the kinetics of cell surface electrochemistry.

The remaining parameters of the periodic pulse signal determine the magnitude of the net change in, for example, the surface concentration of a specifically adsorbed ion or dipole. It is clear that *net* current flow can

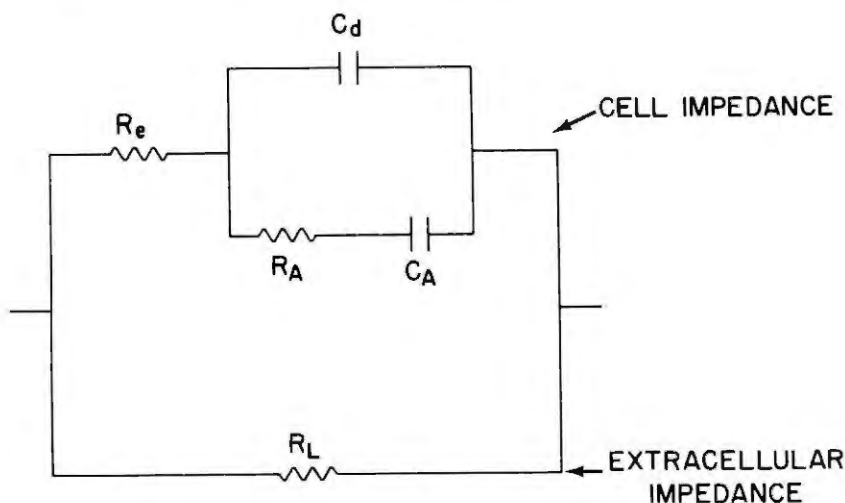


Figure 12-2. Aperiodic electrical equivalent circuit representing the parallel combination of cell membranes impedance with associated cytoplasmic resistance (R_e) and extracellular electrolyte pathway (R_L). The complete cell is represented by a homogeneously distributed dielectric membrane capacitance (C_d) and a specific adsorption pathway (R_A/C_A), which has been experimentally determined to be predominant at short times (high frequencies). Consideration of the complete cell requires that the resistance of electrolyte enclosed by its membrane (R_e) be taken into account.

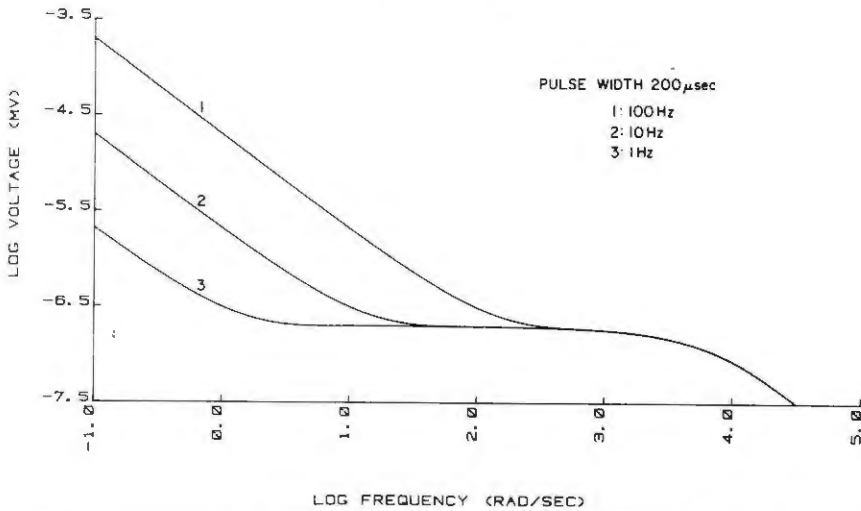


Figure 12-3. Frequency analysis along the real axis (σ) of the Laplace plane illustrating the effect of repetition rate for a unipolar pulse according to equation 6. Note that the primary effect is over the low frequency ($<10^2$ rad/sec) range. This illustrates the manner by which the periodicity of an induced current signal can achieve a net change in the cell's ionic (or dipole) boundary conditions.

increase with repetition rate. This can be shown quite readily by considering the application of a pulse of amplitude having width (τ) and period (T) to a pure resistor (R). The current that flows [$I(s)$] is given by:

$$I(s) = \frac{V}{R} \frac{1 - e^{-\tau s}}{1 - e^{-Ts}} \quad (6)$$

It can be seen that, for a given value of s (complex frequency) and τ , $I(s)$ increases as $T \rightarrow \tau$ and decreases as $T \rightarrow \infty$, reaching its limiting value for a single pulse. An example of the effect of repetition rate is shown by the frequency analysis according to equation 6 given in Figure 12-3. Here amplitude due to variations in T occurs over the low frequency ($<10^2$ rad/sec) portion of the spectrum. The effect of repetition rate variation would therefore be expected to alter the value of the net perturbation of the cell surface process (see equation 3) and represents a convenient manner to obtain a "dose" response for the modulation of cell function. However, it is important to point out that the potential dependence of all cell surface electrochemical processes must be taken into account. When current is applied externally to a cell/tissue complex, *all* cells and their myriad of surfaces and junctions will be exposed to the perturbation. Selectivity in response would appear to depend upon two factors. The first relates to the main activity of the biological system. For example, if growth or repair (response to trauma) constitute the prevalent functional activity, it is probable that one major biochemical pathway is involved for a given

subset of cells (DNA versus RNA or protein synthesis). A biological "window" may therefore be open for perturbation by weak currents if a physical process such as specific adsorption is available. However, several sites involving more than one, e.g. membrane-bound, enzyme could be in the current pathway. Sufficient simultaneous perturbation of all of these could result in cancellation of effect due to counter-regulatory mechanisms. This leads to the second criterion for selectivity in response, which relates to the use of minimum pulse amplitude to obtain the desired effect. The rationale is that the *rate* of activity of regulatory enzymes participating in the functional process, for which the biological "window" is open, is more susceptible to modulation than that of those enzymes that are present (and "inactive" for other functional pathways. Effective amplitudes for perturbation by weak pulsating current are directly dependent upon signal repetition rate (see equation 6). Thus, for a given effective net perturbation, smaller real-time pulse amplitudes are required as signal repetition rate increases. It would appear desirable, therefore, to employ periodic signals with as large a duty cycle as possible.

The above discussion sets forth the general criteria for the choice of pulsating current waveform parameters with the postulate that cell surface electrochemistry is the primary physical process to which these currents will couple. It is not possible to know which particular biochemical process is involved, only that if it contains a surface step, such as specific adsorption, it can be responsive to charge input. Adaptive impedance variations due to the changing extracellular ionic environment (35) modify the value of some of the cell's real-time current pathways. In addition, it is possible that several interfacial enzyme steps are involved in the major functional activity of the cell/tissue complex. Each of these may have different potential dependencies and kinetics, with the result that several net perturbation levels may be effective for modulation of the cell's function. The outcome of this is the expectation that multiple signal encoding may well be the ultimate modality by which the most effective approach to the study and manipulation of cell regulatory processes using weak pulsating currents can be carried out.

Inductive Current Coupling for the Modulation of Cell Surface Electrochemistry

In order to generate a voltage (current) in tissue it was first decided that the induced waveform should have basically rectangular characteristics. This resulted from the kinetic analyses (given above), which show that excitation of real-time charge interactions can be more selectively accomplished if the driving voltage is relatively constant during the perturbation. In addition, the fact that inductive coupling can result in a bipolar waveform has to be taken into account.

The induced current waveform parameters are directly related to the electrical characteristics of the coil. The constancy of these parameters in space depends upon the overall coil/tissue geometry as will be seen below. For any coil the induced electromotive force (emf) is proportional to the rate of change of current in the coil (dI_{coil}/dt). The evaluation of this quantity for a given coil perturbation results in a description of the *shape* of the induced waveform in vacuum, air, and all nonmagnetic homogeneous conducting media in which the resulting current flow is not high enough to produce sufficient back emf for phase relationships to cause a waveform modification.

Coil current [$I_{coil}(t)$] for an air core inductor is, for a voltage step (V_o):

$$I_{coil}(t) = \frac{V_o}{R_{coil}} \left[1 - \exp\left(-\frac{tR_{coil}}{L}\right) \right] \quad (7)$$

where L is the coil inductance and R_{coil} is the effective coil resistance, including all connecting cable and driving circuit resistances. Equation 7 shows that $I_{coil}(t)$ rises exponentially to the short circuit value (V_o/R_{coil}) at a rate determined by the coil time constant, ($\tau_{coil} = L/R_{coil}$). As mentioned above, the *waveform* of the induced voltage is a direct function of the time derivative of equation 1, which is

$$\frac{dI_{coil}}{dt} = \frac{V_o}{L} \exp\left(-\frac{tR_{coil}}{L}\right) \quad (8)$$

Equation 8 clearly shows that in order to achieve a rectangular type induced waveform, at least in one polarity, τ_{coil} should be greater (by 10 times) than τ_{cell} . This can be achieved by the proper choice of L and R_{coil} . One modality is to keep L relatively small so that safe driving voltages (<25 V) can be employed. Note that, as given by equation 8, the maximum induced voltage (as $t \rightarrow 0$) is inversely proportional to coil inductance for a given V_o . Effective coil resistance can be kept small by utilizing heavy magnet wire and connecting cable (14 to 16 B&S gauge). With the above taken into account it is easy to see that, for a given Γ_{coil} , the voltage step (V_o) can be applied to the coil for as long a time as the following relation is approximately valid:

$$\left(\frac{dI_{coil}}{dt}\right)_{t \rightarrow 0} = \frac{V_o}{L} \left(1 - \frac{tR_{coil}}{L}\right) \quad (9)$$

Over the time during which equation 9 holds, an induced voltage waveform in the form of a "step" having some negative slope will be achieved.

In order to maintain the relative rectangular nature of the induced voltage while the coil is being activated and to avoid excessive current utilization (see equation 7 for $t \rightarrow \infty$), the coil driving voltage (V_o) is abruptly turned off well before τ_{coil} is satisfied. The time during which the coil is under active excitation is thus determined by the time interval over which equation 9 is approximately valid. At the time of coil turn-off (t_f) the stored

“magnetic” energy must be recovered (assuming no heat loss). This can be achieved in either of two manners. In the first, the coil current is allowed to decay at a rate determined only by the coil inductance, effective resistance, and maximum allowable opposite polarity voltage swing. In the second, this voltage swing is amplitude-limited by diode. By using either of the above modes, induced waveform patterns having different opposite polarity time and amplitude asymmetry can be achieved. By choosing a relatively low coil inductance, the magnetic field can be made to collapse over a time interval that is usually significantly shorter than the coil activation time. In essence, when the coil driving voltage (V_o) (see equation 9) is removed at t_f , the following relation holds:

$$V(t = t_f) = I(t_f) \times (R_{coil} + R_{switch}) + V(t_f) \delta(t) \quad (10)$$

which states that, at the instant of coil turn-off, the voltage [$V(t = t_f)$] attempts to achieve a value of infinity [as described by the delta function, $V(t_f) \delta(t)$] of polarity opposite to that of V_o (i.e. the magnetic field will start to collapse). Although this instantaneous delta function of voltage adds to that generated by $I(t_f)$ as it commences to flow through the effective coil resistance that now includes the switch resistance (R_{switch}), switching time in practice is significantly longer than the time during which $V(t_f) \delta(t)$ can be developed. Therefore the driving voltage at $t \sim t_f$ at the start of magnetic field collapse is, for all practical purposes, given by: $I(t_f) \times (R_{coil} \times R_{switch})$. In practice R_{switch} can be made voltage dependent with the result that the total time for magnetic field collapse can be made variable. The result is that, to a first approximation, for $t \geq t_f$:

$$\frac{dI_{coil}}{dt} = \frac{I(t_f) \times (R_{coil} + R_{switch})}{L} \exp\left(-\frac{t(R_{coil} + r_{switch})}{L}\right) \quad (11)$$

Inspection of equation 11 shows that, for $R_{switch} \gg R_{coil}$ (a condition always achieved in practice for this modality), both the driving voltage and the time constant associated with the collapse of the magnetic field are much larger and much smaller, respectively, than the same parameters for coil excitation (i.e. during the rise of the magnetic field).

The induced voltage waveform under the above conditions is a direct function of equation 8 for $t < t_f$ and equation 11 for $t > t_f$. A schematic illustration of this is shown in a, Figure 12-3.

As indicated above it is possible to obtain quite another time/amplitude asymmetry relationship for the induced waveform by placing a diode in parallel with the coil(s) utilized. Under these conditions, the opposite polarity voltage swing at $t = t_f$ is limited to a fraction of V_o (the coil driving voltage) and the opposite polarity voltage ($-V_{coil}$) is practically instan-

taneously clamped to the forward diode voltage. The induced voltage waveform (for $t > t_f$) is now directly related to:

$$\frac{dI_{coil}}{dt} = -\frac{V_{coil}}{L} \exp\left(-\frac{t(R_{coil} + R_{diode})}{L}\right) \quad (12)$$

Since $-V_{coil}$ is much smaller than V_o (see equation 8), the induced voltage at $t = t_f$ is correspondingly much smaller than that as $t \rightarrow 0$. In addition, since R_{diode} (when conducting) is never larger than R_{coil} , and usually ten to one hundred times smaller, the collapse of the magnetic field will be governed essentially by the original coil time constant ($\tau_{coil} = L/R_{coil}$). Therefore the total duration of the opposite polarity portion of this waveform type is significantly longer than that of its primary polarity. This is illustrated in b, Figure 12-4.

The waveforms obtained by the procedure just described represent the dynamics of the current signal, which is applied to the extracellular fluid/cell complex. The distribution of current flow depends upon the geometry of coil and tissue. The basic rule is that the voltage induced will act like a voltage source, the terminals of which are defined by the distribution of magnetic flux within the tissue. Thus, the induced voltage field (E) around

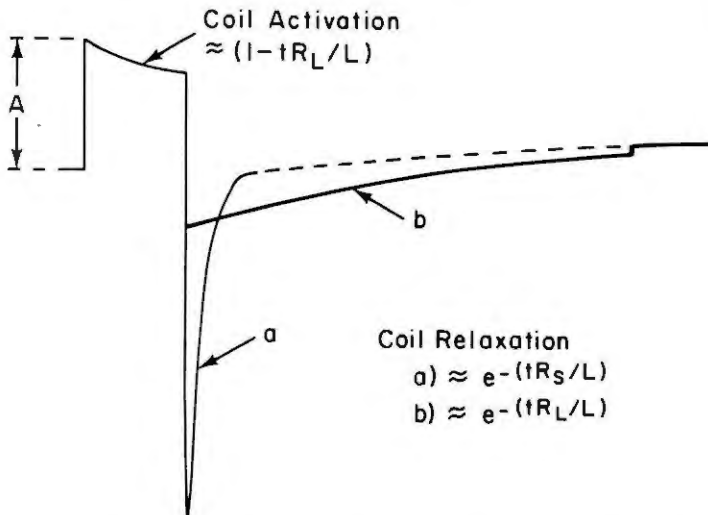


Figure 12-4. Schematic illustration of the inductively coupled current waveform used in this study. The coil time constant (L/R_L) determines the shape of this signal during activation and the duration of a diode limited opposite polarity signal (b) during coil relaxation (magnetic field collapse). In the absence of a diode, the curve is primarily determined by the electronic driving circuitry (a). Both (a) and (b) time-amplitude asymmetry contribute to the quantitative description of the signal/biological effect correlation described in this work.

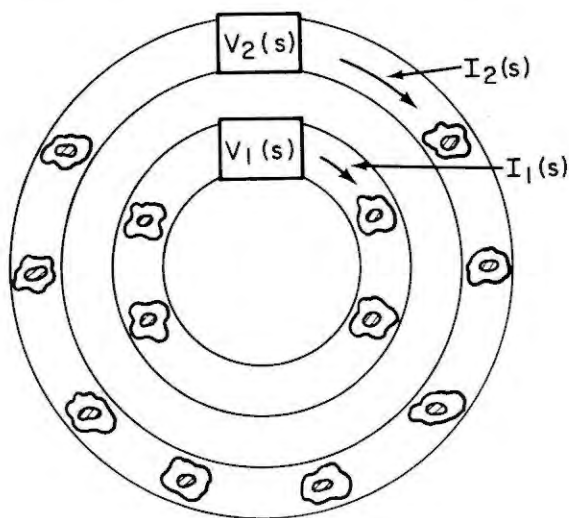
a loop of length (l) is related to the spatial distribution of the magnetic field (B) over a surface of area, (A) by:

$$\oint E dl = - \frac{d}{dt} \int_s B dA \quad (13)$$

Using equation 13, the dynamic induced voltage [$V(s)$] expressed in the complex frequency domain is obtainable for the generally cylindrical geometry of the magnetic field between facing planar circular coils as

$$V(s) = -K\pi r^2 sB(s) \quad (14)$$

where K is the coil coordinate system constant, r an arbitrary loop radius within the homogeneous magnetic field, and $B(s)$ is proportional to equation 9 for coil activation and either equation 11 or 12 for coil relaxation (magnetic field collapse). It is obvious from equations 13 and 14 that the amplitude of the voltage source [$V(s)$], depends upon the size of the loop around which it is considered to act. The important variable, however, is the current that results. To estimate its distribution, the physical picture



$$V_2(s) = 2 V_1(s)$$

$$Z_2(s) = 2 Z_1(s)$$

$$I_2(s) = I_1(s)$$

Figure 12-5. Illustration of one possible mode by which uniform current distribution can be induced in a relatively homogeneous cell/extracellular fluid mixture. Electromagnetically induced voltage sources [$V_1(s)$, $V_2(s)$] have values determined by the spatial distribution of the magnetic field. If the impedance pathway of the cell/electrolyte combination [$Z_1(s)$, $Z_2(s)$] has similar geometric dependence, current flow around each induced voltage loop [$I_1(s)$, $I_2(s)$] will be approximately identical.

shown in Figure 12-5 can be considered. Here a relatively homogeneous arrangement of cells within the conducting extracellular medium is considered as a first approximation. Under these conditions, the impedance around any loop defining the amplitude of the induced voltage source increases linearly with loop diameter. The result is that the induced current "seen" by each cell in the relevant tissue area is relatively constant, provided that the magnetic field is spatially homogeneous. Note that the low impedance pathways (as $s \rightarrow \infty$) defined in the cell surface model given above make the direction of current flow relatively unimportant. This is so since the supposed electrochemical processes do not behave as distributed parameter systems (31, 36), i.e. their *relative* positions are not critical. This would not be the case if the current pathway were restricted to the external cell surface (1).

Relation Between Waveform Configuration and Biological Effect

It is important at the onset to remember that the class of physical processes to which the weak pulsating current waveforms of the present study are designed to couple do not represent the overall metabolic activity of a cell. Rather, the step involved is a physicochemical one that is informational or catalytic in nature. Thus these weak currents do not supply the energy for a particular biochemical process. In this context the analysis to be given here attempts to consider real-time electrochemical response as providing a net change in cellular boundary conditions.

In order to quantitatively describe the variety of waveform configurations that can be obtained via inductive coupling, it is obvious that frequency analysis of the perturbation signal can be a powerful tool. For this, real axis Laplace transformation has been employed. The methodology has been described in detail elsewhere (47, 48). Briefly, however, the frequency spectrum of any time function $[f(t)]$ can be evaluated according to:

$$F(s) = \int_0^{\infty} f(t)e^{-st} dt \quad (15)$$

where $F(s)$ is the frequency domain function obtained after operating upon $f(t)$ as described by equation 15. When s is replaced by σ , $F(\sigma)$ is a real function that can be readily evaluated using digital techniques. For example a simple pulse having duration ($T1$) and amplitude (V) has the frequency function:

$$F(s) = \frac{V}{s} [1 - \exp(-sT1)] \quad (16)$$

The basic bipolar pulse configuration shown in a or b, Figure 12-4, has a frequency spectrum defined by:

$$F(s) = \frac{A}{s} [1 - \exp(-sT1)] - \frac{T1}{T2} [1 - \exp(-sT2)] \exp(-sT1) \quad (17)$$

where T_1 and T_2 are the main and opposite polarity pulse durations respectively, and A is the amplitude of the portion having duration of T_1 . The periodicity of this waveform is taken into account by dividing the right hand side of equation 17 by the factor $[1 - \exp(-sT_3)]$, where T_3 is the signal period (repetition rate). An example of the effect of repetition rate on the frequency spectrum is shown in Figure 12-3 for a simple unipolar pulse. As mentioned above, amplitude over the lower frequency portion of the spectrum increases with repetition rate.

The availability of a large body of data describing the effect of inductively coupled waveforms in both in vitro and in vivo systems has allowed an attempt at waveform/biological effect correlation on the basis of equation 17 coupled with periodicity (and burst configuration in a similar manner). The curves shown in Figure 12-6 were obtained for two bursts and one single pulse configuration (as described). All of which had nearly identical biological effect in at least two systems (22, 23, 46). As can be seen, there is no frequency region over which any obvious amplitude correlation exists. This is not entirely unexpected if the electrochemical information transfer concept is valid. In other words the cell surface process must also be taken into account. This can be performed for any of the electrochemical steps

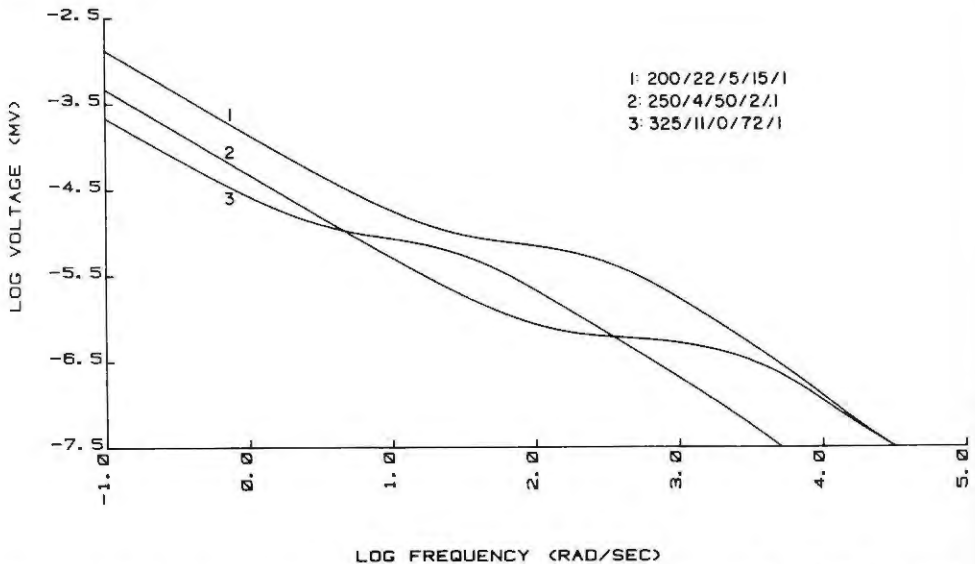


Figure 12-6. Laplace plane frequency analysis of electromagnetically induced voltage signals according to equation 17. Numbers in legend for each curve refer to (from left to right): main and opposite polarity pulse width (μsec); burst width (msec); repetition rate (Hz); and amplitude (refer to Fig. 12-4 and text for explanation of calibration; amplitude units are arbitrary and should be used for comparison only). Waveforms analyzed have triggered similar biological effect in several in vitro and in vivo systems. Note that amplitude correlations do not exist over any frequency range for all three signals.

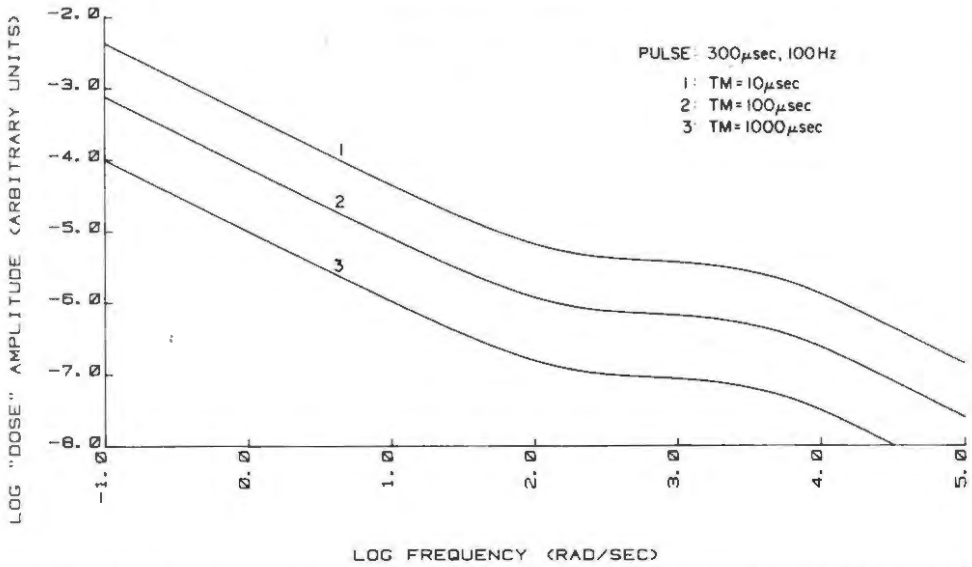


Figure 12-7. Real axis Laplace frequency analysis for a unipolar pulse assuming a specific adsorption current pathway at the cell surface having the indicated relaxation times. These curves illustrate the "dose" amplitude perceived by the cell as a function of the kinetics and irreversibility (nonlinearity) of this electrochemical process.

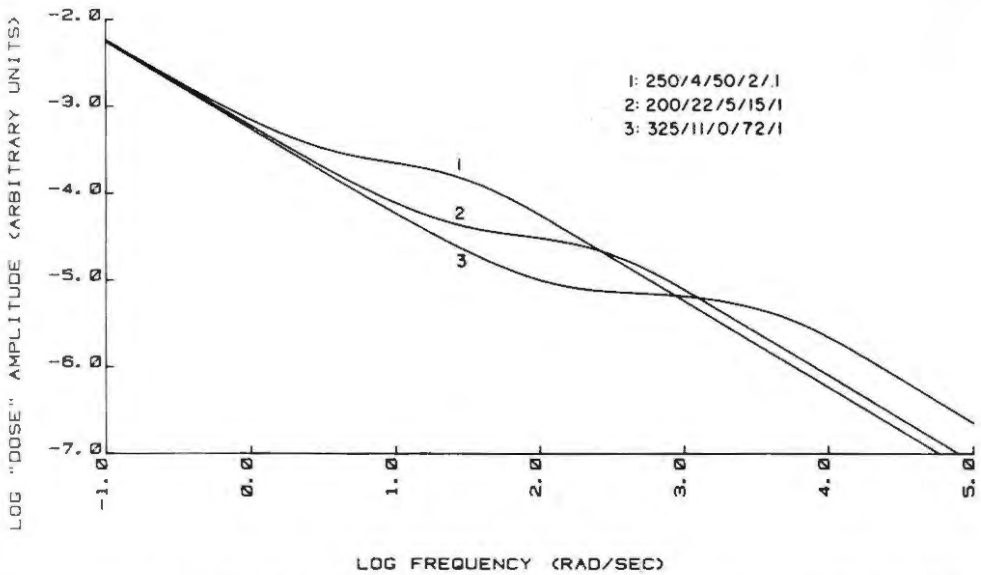


Figure 12-8. Spectral analysis as in Figure 12-7 for the waveforms indicated in Figure 12-6. Addition of cell surface model with relaxation time in the 10 μ sec range results in "dose" amplitude correlation over low frequency range (rad/sec) of spectrum, indicating that nonlinearity of electrochemical response may be the mechanism by which modulation of cell function is attained using weak periodic currents.

(or combination thereof) described above. For reasons that will become apparent below, the preferred pathway is that involving specific adsorption. In this case both the kinetics and irreversibility of the process are taken into account by considering that the net change $[\Delta P(t)]$ — in for example, surface concentration of a specifically bound ion or dipole — can be described as:

$$\Delta P(t) = \frac{TM1}{T1} [1 - \exp(-T1/TM1)] + \frac{T1 \times TM2}{T2} [1 - \exp(-T2/TM)] \quad (18)$$

where $TM1$ and $TM2$ represent the forward and reverse relaxation times respectively, and $T1$ and $T2$ the durations over which these are excited by the average value of each polarity of the basic signal. Equation 18 defines the average perturbation caused by each pulse. Periodicity and burst mode contribute in a manner similar to that for the input waveform alone. Use of this model dependent analysis readily allows the basic relaxation time of the cell surface process to be taken into account. The effect of the predominant time constant ($T1$) using a single bipolar repetitive pulse is shown in Figure 12-7. The effect of $T1$ on the average perturbation ("dose" amplitude) is evident. An important consequence of this approach is the ability to correlate basic pulse durations and periodicity versus $TM1$ and $TM2$ to ascertain (a) existence of correlation versus biological effect and (b) frequency range over which the correlation exists. The curves shown in Figure 12-8 were calculated for the same waveforms utilized to obtain Figure 12-6 using $TM1$ and $TM2$ in the 10 μ sec range (with 10% nonlinearity). As can be seen, the "dose" amplitude for each waveform is nearly identical over the low frequency portion of spectrum. Note that the biological effect of these signals was nearly identical in at least two systems, indicating a remarkable correlation between the kinetics of the waveform/cell surface process combination and the catalytic effect elicited. The observation that correlation exists over the low frequency region is indeed an important one, since it provides strong circumstantial evidence that the design of signals to couple to the kinetics of cell surface electrochemistry can act via an informational mode. It is to be remembered, however, that basic pulse duration is limited by the presence of the extracellular ionic current pathway (see equation 5).





A systematic experimental verification of the correlation of induced current waveform parameters has recently been reported (46), and a brief review is given here. The experimental design was simple and consisted of a short term in vitro chondroosteogenic system using total Ca^{++} uptake (via ^{45}Ca) as evidence for the biological effect. Calcium is utilized in a variety of metabolic pathways and in a calcifying system will rapidly exchange with that already bound in the extracellular matrix or in a metabolizing pathway. In addition, the entry (or exit) of Ca^{++} into the cell for

incorporation into pools, such as that involving the mitochondria, may be under enzymatic control, e.g. the membrane-bound Ca-ATPase (49, 50) system. If the activity of this membrane surface process can be modulated by kinetic coupling with induced currents, the effect should be observable as an increase (or decrease) in Ca^{++} uptake versus controls over relatively short times.

For this experiment both tibiae from nine day White Leghorn chick embryos were isolated and individually placed in isotonic salt solution at pH 7.6 (51) containing $0.5 \mu\text{c}$ ^{45}Ca . One tibia from each embryo was exposed to induced current using a pair of $10 \times 10 \text{ cm}$ air gap coils wound with sixty turns of #14 B&S gauge magnet wire, placed 6 cm apart. The contralateral tibia served as control. The coils were powered to obtain the signals described in Table 12-1 using equipment supplied by Electro-Biology, Inc. (Fairfield, N.J.). The amount of ^{45}Ca uptake was assessed at the end of one hour of exposure to induced current by scintillation counting. In this manner the amount of ^{45}Ca remaining in the incubation medium versus $t = 0$ was indicative of active versus control response.

Although this system has been extensively employed for a preliminary evaluation of the biological effect of induced periodic current, only results from variations of two basic waveforms will be discussed here. These are single and burst pulse versions of the signal described in a, Figure 12-4.

TABLE 12-1
EFFECT OF INDUCED CURRENT SIGNAL CONFIGURATION
FOR $10 \mu\text{s}$ REAL TIME CELL SURFACE RESPONSE
(Ca uptake in embryonic chick tibia, $p < 0.001$)

SIGNAL	% INCREASE vs CONTROL	N
<i>Periodic Single Pulse</i>		
 325/12 72Hz A=1	26.6 ± 4.9	12
 50/0.8 150Hz A=1	29.0 ± 6.1	11
<i>Periodic Pulse Burst</i>		
 200/20 5/15 A=1	32.5 ± 5.9	13
 25/0.9 5/35 A=1	34.8 ± 6.1	11

Choice of the basic waveform amplitude (a , Fig. 12-4) was based on experience evolving from the first inductively coupled current signal that was reported capable of accelerating fracture repair *in vivo* (52, 53). At the time of these studies, the waveform parameters that were effective were chosen on the basis of the electrochemical information transfer hypothesis (30, 31) without, however, benefit of the experimental values for cell surface electrochemical kinetics. Amplitudes are calibrated using a search coil consisting of sixty-five turns of #36 B&S gauge magnet wire wound in a plane of 1 cm circumference. The designation $A = 1$ for this study (see Table 12-1) refers to a calibration voltage field having a peak of 1.5 mV/cm as $t \rightarrow 0$ in the loop defined by the search coil circumference. This value depends on the size of the voltage loop and increases with loop diameter. However, the current density will be relatively uniform if the geometric distribution of the cell/extracellular fluid complex is reasonably homogeneous (see Fig. 12-5).

In order to evaluate the actual induced current at the cellular level a relatively simple experiment was performed. The isolated toad urinary bladder placed in the conductivity-type chamber used for impedance measurements (34) was situated between two coils, as shown in Figure 12-9. The chamber is such that any current that flows from, for example, the left to right compartment must pass through a 1 cm² epithelial cell sheet. Carbon electrodes of large surface area (10 m²) were situated in each compartment and connected via a twisted pair of copper wires to a load resistor placed at its termination (see Fig. 12-9). The load resistor was located 3 meters from the coil pair in order to minimize stray induction. A Nicolet® 1090A transient recorder having 100 msec time resolution was utilized to record the voltage drop across a 10Ω load resistor (a value substantially lower than the electrolyte resistance between the flanking electrodes). The experiment thus consisted of a defined current pathway in which a voltage source could be induced via the spatially homogeneous time varying magnetic field existing between a coil pair identical to that employed for the *in vitro* Ca⁺⁺ uptake study described here. A typical result is shown in Figure 12-10 as output from the transient recorder memory. Here the upper trace (I_e) represents the current flow in the absence of the cell sheet and the lower trace (I_M), that in its presence. Note that the peak current (as $t \rightarrow 0$) is identical (as expected) for both cases and within the anticipated value of 1-10 μA/cm². The *shape* of the current waveform in homogeneous ionically conducting medium (upper trace, Fig. 12-9) is identical to that observed with the search coil. This is expected since the induced voltage is applied in this case to a purely resistive load. The induced current waveshape is modified (lower trace, Fig. 12-9) as it passes across the cell sheet due to the electrochemical impedance of the latter. It is for this reason that the value of peak induced current (as $t \rightarrow 0$) is

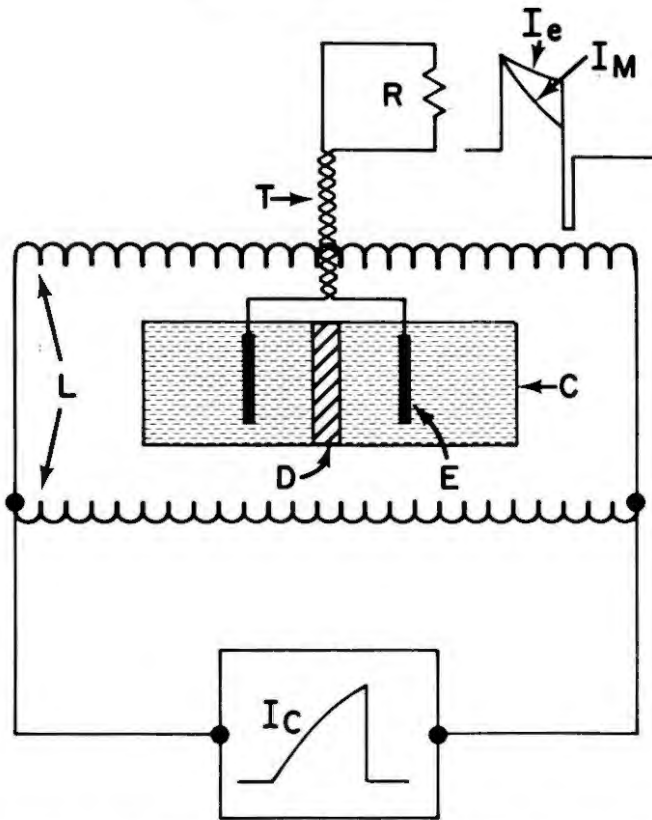


Figure 12-9. Schematic illustration of the experimental apparatus employed for measurement of actual induced current in cell/extracellular fluid complex. The conductivity chamber (*C*) is situated between a coil pair (*L*) producing a spatially uniform magnetic field. The coil driving current (I_c) produces the induced current waveforms (I_e and I_M). Voltage is induced around a loop consisting of a large surface area electrode (*E*) in each compartment of the chamber, isotonic electrolyte, and, when present, an epithelial cell layer at *D*. The current pathway is completed by the resistor (*R*) at the terminal end of a twisted wire pair (*T*). Voltage measurement across *R* allows the magnitude and shape of the induced current waveform to be obtained in the presence (I_M) and absence (I_e) of a tight epithelial cell layer in the current pathway.

given when real-time dosage is considered. Knowledge of average induced current depends upon knowledge of both of the impedance of the cell under study *and* the pathway involved in its relevant regulatory process.

In the context of the Ca^{++} uptake study, the dosage $A = 1$ (see Table 12-1) refers, therefore, to real-time peak induced currents of $1\text{-}10\ \mu\text{A}/\text{cm}^2$. The first waveform employed consisted of a single bipolar pulse having $325\ \mu\text{sec}$ and $12\ \mu\text{sec}$ main and opposite polarity durations respectively, repeating at $72\ \text{Hz}$. A significant 30 percent increase in Ca uptake versus controls was observed (see Table 12-1). Utilizing the frequency analysis

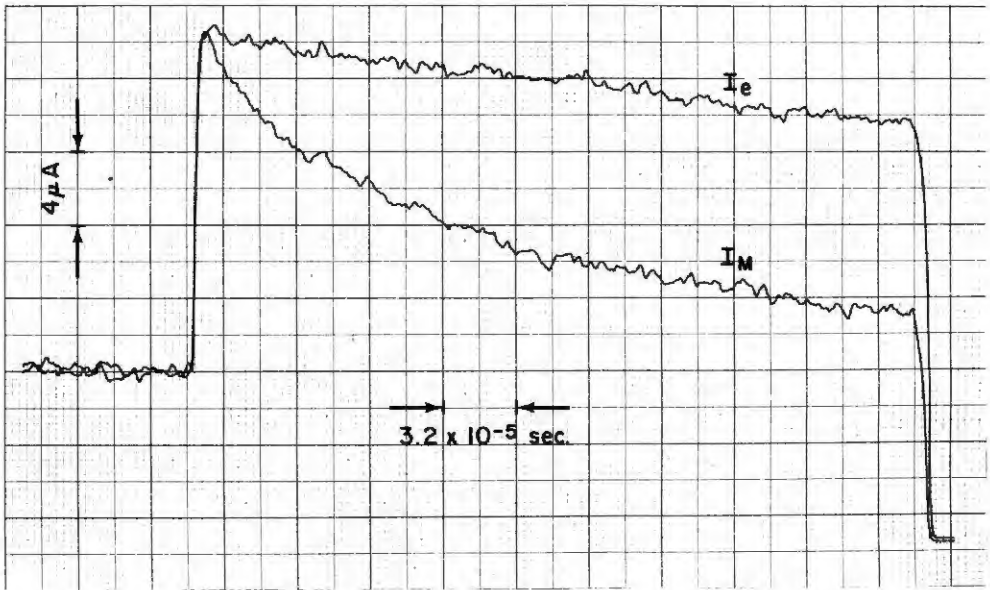


Figure 12-10. Experimental curves representing induced current measured using the apparatus schematized in Figure 12-9. The upper curve (I_e) was obtained in the absence of cells and is identical in *shape* to that observed using a search coil. The lower curve (I_M) shows that effect of the added impedance due to the presence of a cell layer in the current pathway. Note that peak induced current is lower (by approximately 10^3) than that utilized for excitable membrane stimulation.

correlation procedure described above for a specific adsorption pathway having approximately 10 μsec relaxation time, the remaining signals in Table 12-I were predicted to have identical effect. "Dose" amplitude over the low frequency spectral region (see Fig. 12-8) was utilized as the correlation range. The basic waveform variable for both signal types was main polarity pulse duration (T_1) (equations 17 and 18). The rationale for this was an attempt to obtain phenomenological evidence of the possible existence of a cell surface electrochemical process exhibiting specific adsorption functionality and the expected 1-10 μsec time constant, if uncoupled from membrane transport. As seen from Table 12-I, reduction of T_1 from 325 to 50 μsec for the periodic single pulse and from 200 to 25 μsec for the periodic pulse burst only necessitated a factor of 2-3 increase in repetition rate to obtain "dose" amplitude correlations leading to nearly identical increases in Ca^{++} uptake versus controls. Frequency analysis of the input waveform only, via equation 17, predicted a factor of 10-100 increase in repetition rate which, when attempted in this study, failed to affect Ca^{++} uptake.

This study is a preliminary one and was designed to provide evidence of the biological effect of periodic induced current. No biochemical mecha-

nistic interpretations can be extracted from this type of study. However, certain electrochemical mechanistic conclusions can be drawn. The experiment was designed to examine short-term effects, thereby minimizing the adaptive cellular impedance changes that occur as this embryonic tissue differentiates in longer term culture. In addition, variations involving a simple ion were assessed because the anticipated real-time response of this or any biological system is expected to involve entities of this type (31, 54-56). The nature of the electrochemical process that can be excited using weak periodic currents requires pulse durations that correspond to the anticipated (30, 31) and now observed (34, 37, 38) kinetics. This study therefore shows only that the utilization of Ca^{++} can be augmented with the properly tuned current. It cannot provide details concerning which functional pathway is involved. This requires longer term exposure and more specific biochemical tracing. It is, however, intriguing that fracture repair in rats (22), limb regeneration in salamanders (23), and the clinical application to non-union repair (24-26) all exhibit acceleration with a pulse burst waveform (Table 12-1) having (a) main ($T1$) and opposite ($T2$) polarity durations of 200 and 20 μsec respectively, (b) a 5 msec burst width, and (c) repeating at 15 Hz. The low frequency "dose" amplitude for this waveform (see Fig. 12-8) is identical to that for the other three waveforms in Table 12-1.

Mechanism of Biological Action of Weak Periodic Current: A Preliminary View

The approach taken in this study to predict the configuration of weak periodic current signals capable of eliciting biological effect is based on the fundamental hypothesis that non-faradaic electrochemical processes at cell surfaces and junctions are the first "messengers" in the real-time system response (30, 31). The specific pathways possible have been quantitatively modeled and experimentally tested on amphibian epithelial (34) and human red blood cell systems (38). These interfacial kinetic processes require a potential dependent interaction between two specific charged species, one associated with the hydrophilic portions of a membrane or other surface, and the other available in the aqueous phase. The more specific this interaction, the more selective are its possible effects on cell function. The most likely entities involved in the aqueous phase of cell surface electrochemistry are simple ions and large dipoles such as hormones. Because of the more immediate involvement of ions in such processes as repair and development (54-56), it is considered more advantageous to search for the first "messenger" among the various interactions involving ions and regulatory enzymes.

In this context, it is becoming increasingly evident that enzymes regulating the active transport of the ions involved in basic homeostasis are

specifically involved with such fundamental cellular processes as DNA, RNA, and protein synthesis; differentiation; morphological transformation; and respiration (57-61). The most frequently implicated system is membrane-bound Na-K ATPase. If this is indeed the entity involved, it would be expected that extracellular changes in K^+ would have significant effects on the rates of the predominant biochemical pathway to which it is coupled. Convincing proof that Na-K ATPase plays a regulatory role in, for example, DNA synthesis has been obtained through the use of the cardiac steroid ouabain (62). This entity is a very specific inhibitor of Na-K ATPase, acting by competitive adsorption at its extracellular K^+ sites (63).

The relevance of Na-K ATPase to the present study is being assessed using two approaches. The first involves an attempt to identify the molecular origin of the impedance pathway found to be common to the epithelial (34) and human red blood cells (38) and having a specific adsorption functionality (see b, Fig. 12-2). The second involves modulation of Na-K ATPase activity with periodic induced current using a determination of the rate of change of extracellular Na^+ and K^+ concentrations for assessment of effect.

In order to relate the presently understood behavior of the Na-K ATPase system to the interfacial electrochemical considerations of the present study, it is useful to review the effect of extracellular Na^+ and K^+ ion concentrations (64-66). The amount of K^+ influx, expressed per liter of RBC, for a given intracellular Na^+ concentration is dependent upon external K^+ concentration. Generally, the maximal K^+ influx is reached at lower external K^+ concentrations as external Na^+ is reduced. Each curve can be employed to define a half-saturation point, which is interpreted in terms of the number of available extracellular binding sites actually occupied by K^+ . In terms of cell surface electrochemistry, the binding of K^+ and Na^+ to the extra- and intra-cellular sites of Na-K ATPase, respectively, can represent kinetic (specific adsorption) processes responding to weak periodic current. This is particularly true if the degree of effect can be shown to depend upon extracellular K^+ or intracellular Na^+ concentrations. It is to be noted that, when operating stoichiometrically (3 sodium ions out, 2 potassium ions in), the Na-K ATPase sites on the internal membrane surface appear to be highly specific for Na^+ , while those on the outside surface are K^+ specific. It is evident from the above that without resorting to techniques that transiently alter the RBC membrane permeability to increase intracellular Na^+ concentration (67), it is possible to both perform impedance measurements and apply weak inductively coupled current in the presence of altered external Na^+ and K^+ . This has the added advantage of maintaining the RBC relatively intact.

Impedance measurements as described in the previous section have been carried out on the human RBC for different extracellular K^+ con-

centrations. These results, which are preliminary in nature, show clearly that the impedance parameters related to a specific adsorption functionality (R_A, C_A) are modified when external K^+ is 40 times less than normal values (i.e. approximately 100 μM). The results are shown in Table 12-II. It can be seen that the non-specific dielectric membrane capacitance (C_d) remains relatively constant, as expected from the electrochemical surface model described in a previous section. The substantial variations in C_A must be interpreted in light of the altered value of the time constant of the specific adsorption process ($\tau_A = R_A C_A$). Thus, if lowered external K^+ merely resulted in fewer sites occupied, τ_A should have remained constant (i.e. analogous to a surface area change). Clearly, however, the kinetics of binding (related to R_A) are essentially unchanged, whereas the average surface concentration (related to C_A) appears substantially altered. Much more data is required before further quantitative interpretation can be given. It is intriguing, however, to speculate that while C_A may reflect the new number of occupied K^+ sites (dependent upon external Na^+ and K^+), K^+ binding kinetics are more rapid.

The above results point the way toward the use of periodic currents designed to couple to the kinetics of the specific adsorption of K^+ at the extracellular membrane sites of Na-K ATPase. Rate modulation of Na^+ efflux and K^+ influx would provide convincing evidence that a nonfaradaic electrochemical process at the cell surface plays a key role in the regulatory activity of this enzyme. This experiment is described in detail elsewhere (68, 69); preliminary results are briefly given here. The basic study consisted of subjecting fresh human RBC to inductively coupled current utilizing the apparatus described in the previous section. The waveform consisted of 200 μsec main and 12 μsec opposite polarity pulses grouped in a 5 msec burst having an 8 Hz repetition rate. The "dose" amplitude in the low frequency portion of the model-dependent spectral analysis was identical to that shown in Figure 12-8 assuming 10 μsec for the relaxation time of the specific adsorption process (see Table 12-II). Experiments were performed in isotonic Na^+ -free solutions containing 10-300 μM K^+ (i.e. covering approximately one-fourth to full extracellular K^+ site occupation). Changes in extracellular Na^+ concentration were substantial (based on Na-free at $t = 0$), enough to be readily evaluated for

TABLE 12-II
DEPENDENCE OF HUMAN RBC IMPEDANCE ON EXTERNAL K^+ CONCENTRATION

$K^+(\mu M)$	$C_d(F/cm^2)$	$C_A(F/cm^2)$	$R_A(\Omega \cdot cm^2)$
4.0	0.147 \pm 0.021	0.0788 \pm 0.0163	132 \pm 41
1.0	0.155 \pm 0.028	0.0723 \pm 0.0157	141 \pm 43
0.1	0.150 \pm 0.022	0.0381 \pm 0.0134	130 \pm 36

TABLE 12-III
ELECTRICAL MODULATION OF NA-K ATPASE ACTIVITY IN THE
HUMAN RED BLOOD CELL
40 Minute Exposure to Periodic Pulse Burst

K^+ (μM)*	% vs. Control
10	72 \pm 4.9
50	41 \pm 2.3
100	23 \pm 1.6
300	11 \pm 0.7

* K^+ concentration is extracellular at $t = 0$

exposures of less than one hour. Na^+ was determined using an ion specific electrode. Preliminary results are shown in Table 12-III for forty minute efflux times. As can be seen, the effect of periodic induced current on the rate of Na^+ efflux is marked, particularly for low extracellular K^+ concentrations. Little effect is observed at 300 μM K^+ , which corresponds to near saturation of extracellular Na-K ATPase sites. It would appear, therefore, that induced periodic current indeed modulates the rate of activity of this membrane-bound enzyme. More importantly, the effect is observed only when the enzyme is not already operating at maximum rate (i.e. when all K^+ sites are occupied).

The above result, coupled with the observation that a similar impedance pathway (R_A, C_A) exists for two widely different cell systems, leads naturally to the speculation that the Na-K ATPase enzyme is part of the living cell's regulatory process at a very basic level. It is entirely conceivable that the similarity of "dose" amplitude correlations, when widely different induced current waveforms are employed, for a variety of in vivo and in vitro systems, is related to the modulation of Na-K ATPase activity. Clearly an electrical "window" should exist (as reported elsewhere in this volume) related to the required degree of acceleration of enzyme activity commensurate with the cell's functional status. In addition, coupling of Na-K ATPase activity with function would predict the existence of a biological "window" outside of which the cell would be refractory to induced current perturbation. Evidence for this is provided in studies concerning amphibian RBC functional responses to trauma (20, 21). It would in fact be consistent with observations to date that a dynamic (as opposed to steady-state) situation, such as that present in growth and repair, is required for weak periodic currents designed to couple to cell surface electrochemistry to elicit a meaningful biological effect.

REFERENCES

1. Adey, W. R.: *Proceedings IEEE*, 68:119, 1980.
2. Burr, H. S. and Hovland, C. I.: *Yale J. Biol. Med.*, 9:541, 1937.

3. Rose, S. M.: *J. Morphol.*, 77:119, 1945.
4. Smith, S. D.: *Anat. Rec.*, 158:89, 1967.
5. Fukada, E. and Yasuda, I.: *J. Phys. Soc., Japan*, 12:1158, 1957.
6. Becker, R. O.: *J. Bone and Joint Surg.* 43A:643, 1961.
7. Bassett, C. A. L. and Becker, R. O.: *Science*, 137:1063, 1962.
8. Cochran, G. V. B.; Pawluk, R. J.; and Bassett, C. A. L.: *Clin. Orthop.*, 58:249, 1968.
9. Black, J. and Korostoff, E.: *Ann. N.Y. Acad. Sci.*, 238:95, 1974.
10. Marino, A. and Becker, R. O.: *Calc. Tiss. Res.*, 14:327, 1974.
11. Bassett, C. A. L.; Becker, R. O.; and Pawluk, R. J.: *Nature*, 204:652, 1964.
12. Brighton, C. T.; Friedenberg, Z. D.; Zemsky, L. M.; and Polis, R. R.: *J. Bone and Joint Surg.*, 58A:368, 1975.
13. Dwyer, A. F. and Wickham, G. G.: *Med. J. Australia*, 1:73, 1974.
14. Jorgensen, T. E.: *Acta Orthop. Scandinav.* 43:421, 1972.
15. Becker, R. O. and Spadaro, J. A.: *J. Bone and Joint Surg.*, 60A:871, 1978.
16. Bassett, C. A. L. and Herman, I.: *J. Cell Biol.*, 39:9a, 1968.
17. Rodan, G. A.; Bourrett, L. A.; and Norton, L. A.: *Science*, 199:690, 1978.
18. Brighton, C. T.; Cronkey, J. E.; and Osterman, A. L.: *J. Bone and Joint Surg.*, 58A:971, 1976.
19. Shteyer, A.; Norton, L. A.; Pilla, A. A.; and Rodan, G.: 5th International Symposium on Bioelectrochemistry, Weimar, East Germany, Sept. 1979.
20. Chiabrera, A.; Hinsenkamp, M.; Pilla, A. A.; Ryaby, J.; Ponta, D.; Nicolini, C.: *J. Histochem. and Cytochem.*, 27:375, 1979.
21. Chiabrera, A.; Hinsenkamp, M.; Pilla, A. A.; and Nicolini, C.: In *Chromatin Structure and Function*. Nicolini, C., ed. New York, Plenum Press, 1979, p. 811.
22. Chapter 12, this volume.
23. Chapter 8, this volume.
24. Bassett, C. A. L.; Pilla, A. A.; and Pawluk, R. J.: *Clin. Orthop.*, 124:117, 1977.
25. Bassett, C. A. L.; Mitchell, S.; Norton, L.; and Pilla, A. A.: *Acta Orthop. Belg.*, 40:706, 1978.
26. Bassett, C. A. L.; Mitchell, S. N.; Norton, L.; Caulo, N.; and Gaston, S. R.: In *Electrical Properties of Bone and Cartilage*, Brighton, C. T.; Black, J.; and Pollack, S. R., eds. New York, Grune and Stratton, 1979, p. 605.
27. Bawin, S. M.; Kaczmarek, L. K.; and Adey, W. R.: *Ann. N.Y. Acad. Sci.*, 247:74, 1975.
28. Bawin, S. M.; Adey, W. R.; and Sabbott, I. M.: *Proc. Natl. Acad. Sci., U.S.A.*: 75:6314, 1978.
29. Gavalas, R. J.; Walter, D. O.; Hamer, J.; and Adey, W. R.: *Brain Res.*, 18:491, 1970.
30. Pilla, A. A.: In Proceedings 7th Intersociety Energy Conversion and Engineering Conf., San Diego, 1972, Amer. Chem. Soc., Washington, D.C., p. 761.
31. Pilla, A. A.: *Ann. N.Y. Acad. Sci.*, 238:149, 1974.
32. Pilla, A. A.: *Bioelectrochem. and Bioenergetics*, 1:227, 1974.
33. Becker, R. O. and Pilla, A. A.: In *Modern Aspects of Electrochemistry*. Bockris, J. O'M., ed. New York, Plenum Press, vol. 10, 1975.
34. Pilla, A. A. and Margules, G. S.: *J. Electrochem. Soc.*, 124:1697, 1977.
35. Pilla, A. A.: *Adv. in Chem., A.C.S.*, 188:126, 1980.
36. Pilla, A. A.: In *Electrical Properties of Bone and Cartilage*. Brighton, C. T.; Black, J.; and Pollack, S. R., eds. New York, Grune and Stratton, 1979, p. 455.
37. Margules, G. S.; Doty, S. B.; and Pilla, A. A.: *Adv. in Chem., A.C.S.*, 188:108, 1980.
38. Schmukler, R. and Pilla, A. A.: *J. Electrochem. Soc.*, 127:130C, 1980.
39. Cole, K. S. and Cole, R. H.: *J. Chem. Phys.*, 9:341, 1941.
40. Schwan, H. and Cole, K. S.: In *Medical Physics*, vol. 3. Chicago, The Year Book Medical Publishers, Inc., 1960.

41. Schwan, H.: *Adv. Biol. Med. Phys.*, 5, 1957.
42. Plonsey, R.: *Bioelectric Phenomena*. New York, McGraw Hill, 1969, p. 124.
43. Blinks, L. R.: *J. Gen. Physiol.*, 13:361, 495, 1930.
44. Kao, C. Y.: *Gen. Physiol.*, 40:107, 1956.
45. Cole, K.S.: *Membranes, Ions and Impulses*. Berkeley, Univ. of Calif. Press, 1972.
46. Pilla, A. A. and Colacicco, G.: *J. Electrochem. Soc.*, 127:129C, 1980.
47. Pilla, A. A.: *J. Electrochem. Soc.* 117:467, 1970.
48. Pilla, A. A.: In Mattson, J. S.; MacDonald, H. C.; and Mark, H. B., Jr., eds., *Computers in Chemistry and Instrumentation: Electrochemistry*. New York, Marcel Dekker, 1972, p. 139.
49. Schatzmann, H. J. and Vincenzi, F.: *J. Physiol.*, 201:369, 1969.
50. Lee, K. S. and Shin, B. C.: *J. Gen Physiol.*, 54:713, 1969.
51. Cuervo, L. A.; Pita, J. C.; and Howell, D. S.: *Calc. Tissue Res.*, 7:220, 1971.
52. Bassett, C. A. L.; Pawluk, R. J.; and Pilla, A. A.: *Science*, 184:575, 1974.
53. Bassett, C. A. L.; Pawluk, R. J.; and Pilla, A. A.: *Ann. N.Y. Acad. Sci.*, 238:242, 1974.
54. Barth, L. G. and Barth, L. J.: *Develop. Biol.*, 20:269, 1969.
55. Whitfield, J. F.; Rixon, R. H.; McManus, J. P.; and Balk, S. D.: *In Vitro*, 8:257, 1973.
56. Becker, R. O.; Bachman, C. H.; and Friedman, H.: *N.Y. State J. Med.*, 62:1169, 1962.
57. Kaplan, J. G.: *Ann. Rev. Physiol.*, 40:19, 1978.
58. Quastel, M. R. and Kaplan, J. G.: *Nature*, 219:198, 1968.
59. Kay, J. E.: *Exp. Cell Res.*, 71:245, 1972.
60. Smith, J. B. and Rozengwit, E.: *Proc. Natl. Acad. Sci., U.S.A.*, 75:5560, 1978.
61. Koch, K. S. and Leffert, H. L.: *Cell*, 18:153, 1979.
62. Skou, J. C.: *Biochem. Biophys. Acta*, 42:6, 1960.
63. Ledbetter, M. L. S. and Lubin, M.: *Exp. Cell Res.*, 105:223, 1977.
64. Sachs, J. R. and Welt, L. G.: *J. Clin. Invest.*, 46:65, 1967.
65. Garay, R. P. and Garrahan, P. J.: *J. Physiol.*, 231:297, 1973.
66. Glynn, I. M. and Karlish, S. J. D.: *Ann. Rev. Physiol.*, 37:13, 1975.
67. Garay, R. P. and Meyer, P.: *The Lancet*, Feb. 17, 1979, p. 346.
68. Pilla, A. A. and Gary, K.: *Electrochem. Soc.*, 127:130C, 1980.
69. Monet, J. D.; Goureau, Y.; Bagot, J. L.; Pilla, A. A.; and Assailly, J.: Communication presented at the Electrochemical Society National Meeting, St. Louis, May, 1980.